# Nanomechanical Properties of Polyethylene Glycol Brushes on Gold Substrates

Gheorghe Stan,* Frank W. DelRio, Robert I. MacCuspie, and Robert F. Cook

Ceramics Division, Material Measurement Laboratory, National Institute of Standards and Technology, Gaithersburg, Maryland 20899, United States

Ⓢ *Supporting Information*

ABSTRACT: A necessary step in advancing the use of polyethylene glycol (PEG) surface coatings in critical biotechnological applications such as cancer treatments is to provide direct and reliable nanoscale property characterization. Measurements for such characterization are currently provided by scanning probe methods, which are capable of assessing heterogeneity of both surface coverage and properties with nanoscale spatial resolution. In particular, atomic force microscopy (AFM) can be used to detect and quantify the heterogeneity of surface coverage, whereas atomic force spectroscopy can be used to determine mechanical properties, thereby revealing possible heterogeneity of properties within coatings. In this work, AFM and force spectroscopy were used to characterize the morphology and mechanical properties of thiol-functionalized PEG surface coatings on flat gold substrates in aqueous PEG solution. Thiol-functionalized PEG offers a direct and simple method of attachment to gold substrates without intermediate anchoring layers and therefore can be exploited in developing PEG-functionalized gold nanoparticles. AFM was used to investigate the morphology of the PEG coatings as a function of molecular weight; the commonly observed coverage was in the form of sparse, brushlike islands. Similarly, force spectroscopy was utilized to study the mechanical properties of the PEG coatings in compression and tension as a function of molecular weight. A constitutive description of the mechanical properties of PEG brushes was achieved through a combinatorial analysis of the statistical responses acquired in both compression and tension tests. Such a statistical characterization provides a straightforward procedure to assess the nanoscale heterogeneity in the morphology and properties of PEG coverage.
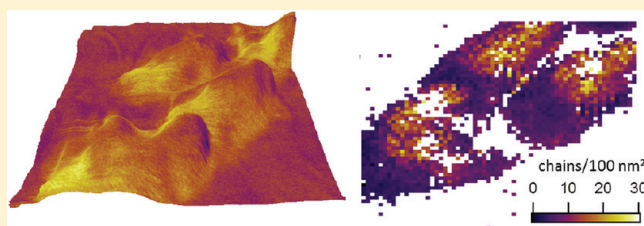
INTRODUCTION

Medical devices have long utilized both gold and polyethylene glycol (PEG) as inert and biocompatible surfaces. More recently, the use of nanomedicine therapeutics, including cancer treatments,[1-4] has combined gold nanoparticles with PEG surface coatings to prevent immune responses.[5-9] A necessary step in advancing the use of PEG surface coatings in such critical biotechnological applications is to provide direct and reliable nanoscale property characterization. For example, measuring the elastic modulus and adhesive properties of PEG surface coatings on nanoparticle surfaces can help model interactions of these nanoparticles with surfaces in the body: The elastic modulus may predict the ability of large polymeric or polymer-coated nanoparticles to be compressed when passing through various pores in the body,[10] whereas the adhesive properties may predict the likelihood of binding to hard surfaces or whether therapeutic targeting molecules have suitable conformational flexibility to bind to the appropriate cellular-receptors.[11] However, to date, no studies have focused on compliant surface coatings on stiff nanoparticle cores, such as PEG on gold. A critical factor in such measurements is an assessment of the homogeneity of both the PEG surface coverage and properties, because these will determine the uniformity of both the immune response and interactions of PEG-coated nanoparticles with their environment. In addition, knowledge of PEG surface coverage and properties will lead to improved models of the fate, transport, accumulation, and excretion of nanoparticle therapeutics. These models could inform therapy-candidate prioritization at the physicochemical characterization stage development, thereby potentially reducing the high costs of toxicity testing numerous formulations.

Many chemical characterization methods have been reported to confirm PEG or thiol-functionalized PEG binding to planar gold and gold nanoparticle surfaces, including infrared spectroscopy,[12] chromatography,[8] and mass spectrometry[9] coupled with digestion of the nanoparticles.[13] However, these techniques are integrative over the entire solution in which the nanoparticles are suspended and thus fail to provide information on the heterogeneity of surface coverage on individual nanoparticles. In addition, these techniques do not provide a direct measure of the physicochemical properties that determine particle interactions with their environment. Consequently, to take full advantage of the therapeutic potential of PEG-coated nanoparticles, it is essential to utilize

techniques that can detect heterogeneity of PEG surface coverage and directly measure PEG properties with single nanoparticle resolution. Scanning probe methods are capable of assessing heterogeneity of both surface coverage and properties with nanoscale spatial resolution;[14] in particular, atomic force microscopy (AFM) can be used to detect and quantify the heterogeneity of surface coverage, whereas atomic force spectroscopy can be used to determine mechanical properties, thereby revealing possible heterogeneity of properties within coatings.

Although several researchers have used the former approach to investigate the heterogeneity of PEG surface coverage,[15−21] only a few have used the latter methodology to assess the heterogeneity of PEG properties.[21,22] Suo et al. investigated the elastic properties of PEG grafted to silicon nitride and gold surfaces in an aqueous solution of potassium chloride and in air.[21] By studying the properties of multiple PEG islands in different environments, the authors showed that the elastic modulus depended strongly on the environment but exhibited only small amounts of heterogeneity within particular islands. Nnebe and Schneider examined the quasi-equilibrium steric forces between unmodified AFM probe tips and PEG grafted to silica surfaces in aqueous PEG solution.[22] These authors demonstrated via contact mode and intermittent-contact mode AFM that the magnitude and spatial decay constant of the steric force depended on the conformation of the PEG molecules (i.e., mushroomlike vs brushlike). In both studies, the mechanical properties of the PEG surface coatings were analyzed only in compression. In addition, in the first study, the elastic moduli of the PEG surface coatings were extracted without taking substrate properties into account, consequently generating artificially inflated values of the coating elastic modulus,[23−25] whereas in the second study, the magnitude and decay constants of the steric forces were not mapped over the PEG surface coating, thus preventing an assessment of the heterogeneity of PEG properties.

In this work, AFM and force spectroscopy are used to characterize the morphology and mechanical properties, in compression and tension, of thiol-functionalized PEG surface coatings on flat gold substrates in aqueous PEG solution. Thiol-functionalized PEG offers a direct and simple method of attachment to gold substrates without intermediate anchoring layers and, therefore, can be exploited in developing PEG-functionalized gold nanoparticles; without an intermediate anchoring layer, the analysis of the mechanical response is also greatly simplified. AFM is used to investigate the morphology of the PEG coatings as a function of molecular weight; the commonly observed coverage was in the form of sparse brushlike islands. Similarly, force spectroscopy is utilized to study the mechanical properties of the PEG coatings in compression and tension. In compression, the PEG coatings are modeled both as discrete PEG molecules forming a brush and as an elastic continuous film. For the continuum analysis, a first-order elastic perturbation method is used to account for substrate effects. In tension, the PEG molecules are modeled as thin, elastic rods with continuous curvature and a characteristic correlation length. Together, the various models are used to map a number of mechanical properties within individual PEG islands of different molecular weight, which enables a statistical approach to assess the heterogeneity of PEG properties.

■ EXPERIMENTAL METHODS

Any mention of commercial products in this article is for information only; it does not imply recommendation or endorsement by the National Institute of Standards and Technology.

Materials. Methoxy-terminated thiolated PEG (CH$_3$O-(CH$_2$CH$_2$O)$_n$ CH$_2$CH$_2$SH, where n is the number of ethylene oxide monomers) with average molecular weights of 5000 Da (PEG 5K, $n \approx 113$) and 20 000 Da (PEG 20K, $n \approx 452$) were purchased from Nanocs (New York, NY) and used as received. The length of the PEG monomer, l, in a good solvent (i.e., a solvent that promotes swelling of a polymer)[26] is $l = 0.424$ nm,[27] giving contour lengths $L_C = nl$, the lengths at maximum chain extension, of 47.9 and 192 nm for PEG 5K and PEG 20K, respectively. The radii of gyration R_g in a "theta" solvent are 1.84 and 3.68 nm for PEG 5K and PEG 20K, respectively; for a theta solvent, $R_g = l(n/6)^{1/2}$.[28] The average polydispersity as reported by the vendor for PEG batches was <1.08. Silicon (100) wafers with a 5 nm Ti adhesion layer and a 100 nm gold film were supplied by Sigma-Alrich (Milwaukee, WI) and cut into 6 mm × 6 mm samples. Sulfuric acid (H$_2$SO$_4$, 95.0−98.0% pure, ACS reagent) and hydrogen peroxide (H$_2$O$_2$, 30.0 wt % in H$_2$O, ACS reagent) were purchased from J. T. Baker (Phillipsburg, NJ) and used as received. All PEG solutions were prepared using deionized (DI) water (resistivity of ≈18.2 × 10^6 Ω cm) from an Aqua Solutions (Jasper, GA) type I biological grade water purification system outfitted with an ultraviolet lamp to oxidize residual organics and a low molecular weight cutoff membrane to remove pyrogens.

Sample Preparation. All sample preparation was performed in a class 10000 clean room at 21 ± 1 °C and 45% relative humidity (RH) ± 5% RH (uncertainties indicate typical daily variabilities). The Au/Ti/Si(100) samples were cleaned with a piranha solution (3:1 H$_2$SO$_4$/H$_2$O$_2$) to remove organic contamination on the gold surface. The samples were then immersed in a 0.2 mM DI water solution of PEG 5K or PEG 20K for 24 h, transferred directly to the AFM fluid cell, and immersed in the aqueous PEG solution. At least three regions on at least three separate sample preparations were examined. Areas were selected arbitrarily, but away from the edges of the samples to avoid potential edge effects. Data presented in figures are representative of all areas examined.

Atomic Force Microscopy. The AFM used in this work was a commercial MFP-3D Asylum instrument (Santa Barbara, CA). Intermittent-contact (tapping) mode AFM was used for topography imaging and force spectroscopy (force-volume mapping) was used for recording the force-displacement response at each node of a square grid (64 × 64) distributed over the investigated area. Each force-displacement measurement consisted of 2048 measurements along the AFM probe approach and retract sections. The AFM was programmed to impose a maximum force and displacement during approach of 8.0 nN and 500 nm, respectively. The AFM probes used for measurements were triangular SiN DNP probes (Bruker, Santa Barbara, CA) with spring constant $k_C = 0.08$ N m^{-1} ± 0.01 N m^{-1}, where the uncertainty represents one standard deviation from multiple measurements. The calibration of the spring constant of the probes was made in air by using the thermal calibration method of the MFP-3D AFM; the optical sensitivity of the AFM system, connecting output voltage to applied force, was assessed in air and adjusted in solution (to preserve the calibration) through force-displacement measurements on a

3139

dx.doi.org/10.1021/jp211256f | J. Phys. Chem. B 2012, 116, 3138−3147

Si(100) surface. The measurements in solution were made in the closed fluid cell of the MFP-3D AFM. For analysis, the measured force-displacement curves on PEG 5K and PEG 20K were converted to force-deformation (F-δ) curves by subtracting the cantilever deflection (F/k_C) from the AFM z-piezo displacement. Models describing the force-deformation response were fit to the F−δ curves at each point in the 64×64 square grid using IGOR Pro (WaveMetrics, Portland, OR), and the resulting fit parameters were used to create both maps and histograms of mechanical properties. After force spectroscopy measurements, the same tip was used to image cylindrical Si nanowires on a flat Si(100) surface. The tip radius, $R_T = 31$ nm ± 5 nm, was determined by considering the tip contribution to the topographical cross section of the imaged nanowire;[29] the uncertainty represents one standard deviation from multiple measurements.

■ RESULTS

PEG 20K and PEG 5K Imaging. The morphology of PEG 20K and PEG 5K on bare gold substrates were investigated by AFM. With both contact mode (not shown here) and intermittent-contact mode (Figure 1) AFM, the commonly
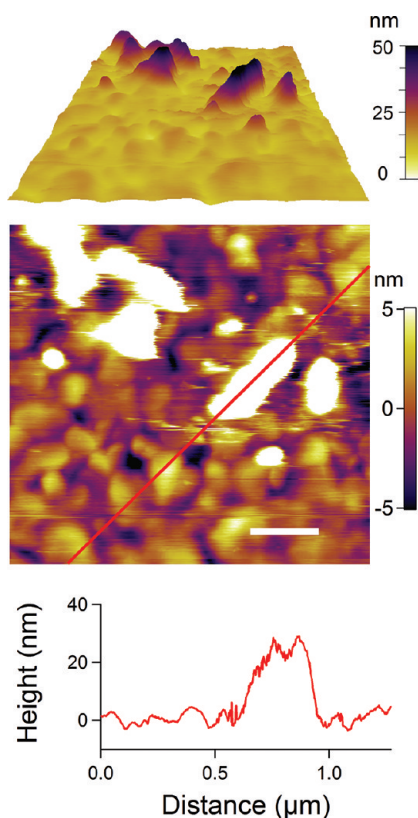

Figure 1. (a) 3D and (b) 2D topography profiles over a 1 μm $\times$ 1 μm area of PEG 20K imaged in aqueous PEG solution. (c) Topographical cross-section profile along the line shown in part b. Scale bar is 200 nm.

observed coverage for both PEG 20K and PEG 5K was in the form of sparse individual brushlike islands up to 500 nm in size. This is in contrast to functionalized surfaces,[15,16,30] which provide uniformly covered areas of densely grafted PEG. Figure 1a shows an example of the three-dimensional (3D) topography of PEG 20K islands. At a smaller z-scale in Figure 1b, a two-dimensional (2D) projection highlights the surface features

and the contours of the PEG islands in aqueous PEG solution. The edges of the PEG islands were not precisely resolved by AFM because of the tip-shape convolution effects and the probable mushroom configuration of the peripheral molecules of these islands. In addition, as suggested by the occasional blurriness in this scan, there were individual PEG chains, either attached to the gold substrate or floating in solution, which could not be resolved individually.

The heights of the PEG 20K islands as measured by intermittent-contact mode AFM were up to 40 nm; a detailed height profile across one of these islands is shown in Figure 1c. Similar measurements showed that the heights of the PEG 5K islands were up to 30 nm. Some samples were removed from the fluid cell and subsequently imaged in air after drying; a dendritic network was observed on the substrate surrounding the original PEG islands. The heights of the original PEG islands were not altered by the drying process, suggesting that the dendrites were the result of crystallization of PEG chains that were initially floating in solution and then dried on the gold surface when the sample was removed from solution (see Supporting Information for additional details). To avoid AFM and force spectroscopy artifacts connected with the dendrites, all subsequent measurements were performed on PEG in solution in the fluid cell.

An example of a 2D image of PEG 5K islands obtained using intermittent-contact mode AFM is shown in Figure 2a and is
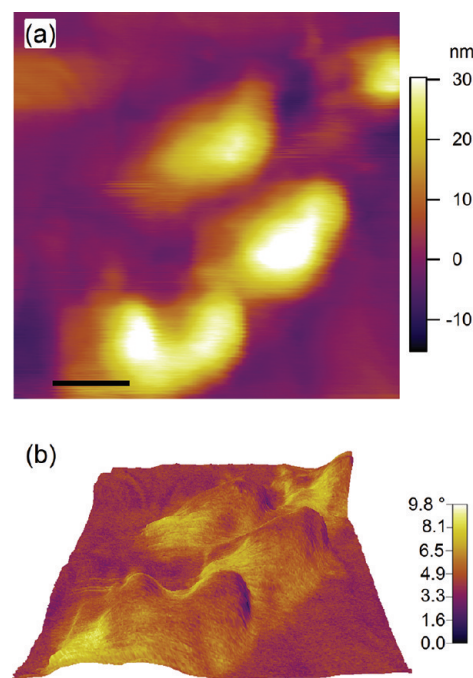

Figure 2. (a) 2D topography profile over a 500 nm $\times$500 nm area of PEG 5K imaged in aqueous PEG solution. (b) The color contrast of the angular phase image was superimposed over the 3D topographical surface to highlight the PEG covered areas. Scale bar is 100 nm.

similar to that of the PEG 20K islands. Figure 2b is a 3D topographic image of the same PEG 5K islands with the angular phase contrast from the intermittent-contact mode AFM superimposed as a color map. The phase contrast highlights the PEG grafted regions relative to the gold substrate within the scanned area, supporting the topographical maps that indicate heterogeneous PEG surface coverage in the form of individual

islands. In addition, the phase contrast within the individual PEG islands varies, providing *qualitative* evidence that the mechanical properties of the PEG brushes within the islands is heterogeneous. To gain *quantitative* insight into the mechanical property heterogeneity, force spectroscopy of individual PEG islands is required. On the basis of the tip radius and maximum force used in this study, contact radii on the order of a few nanometers are anticipated, suggesting that the force spectroscopy measurements should be able to detect heterogeneity of brush mechanical properties within an island.

PEG 20K Force Spectroscopy. The mechanical response of PEG 20K brushes on flat gold surfaces was investigated by mapping the force-deformation response over small areas. Areas 500 nm × 500 nm were imaged to locate PEG islands by intermittent-contact mode AFM. Force spectroscopy was performed over the same areas to measure the mechanical response of PEG during the approach and retract actions of the AFM probe tip. Different force-deformation responses from the force spectroscopy are shown in Figure 3. In Figure 3a, three force-deformation curves are shown, two measured on PEG and one measured on the gold substrate. The curves were aligned horizontally such that the upper, substrate contact, sections of the responses were aligned and then separated
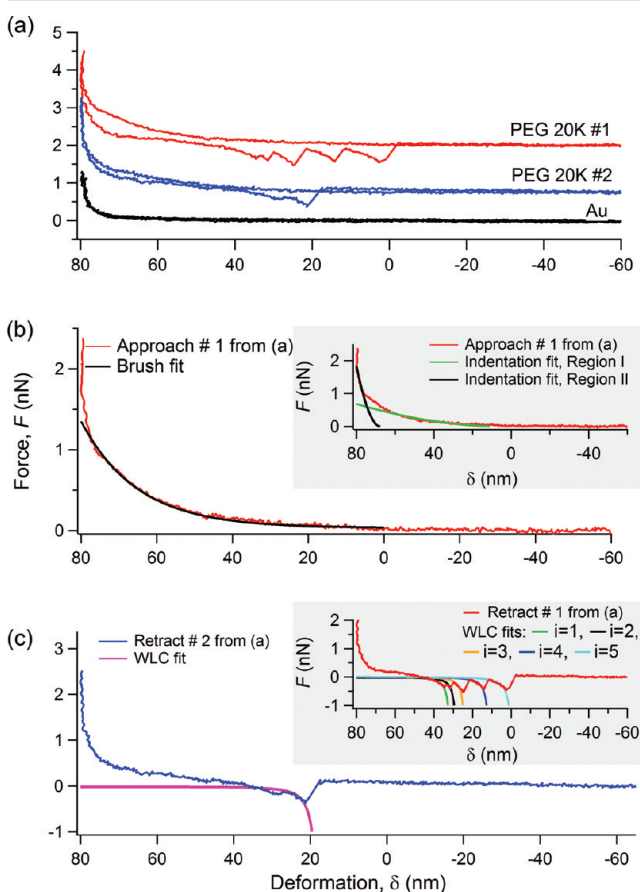

Figure 3. (a) Force-deformation curves on PEG 20K and the bare gold substrate in solution; the curves were aligned horizontally such that the upper, substrate contact, sections of the responses were aligned, and then separated vertically for clarity. (b) The approach section of curve 1 is analyzed in terms of the Alexander−de Gennes brush model and the Xu and Pharr film−substrate model (inset). (c) The retract sections of curve 1 (inset) and curve 2 are analyzed in terms of the WLC model.

vertically for clarity. The ordinate axis is for the gold measurement; the abscissa axis is from a fit to a PEG measurement, as discussed below.

Distinct features are observed in the AFM probe's deflection, and thus imposed force, on both approach and retract sections of the two PEG curves, giving rise to contact hysteresis loops not observed on the bare gold. On the approach section, an enhanced repulsive (positive) force between the AFM probe tip and substrate, commonly 80 to 90 nm before substrate contact, was observed. On the retract sections, an attractive (negative) force between the probe and substrate, commonly extending about 50−80 nm from the substrate, sometimes exhibiting multiple instabilities, was observed.

Three models were used to analyze the mechanical responses of PEG surface coatings in compression and tension—two models for compression and one model for tension. The three models are originally based on, or slightly modified to be described in, an indentation-type coordinate system (i.e., the inward normal to the indented system is positive,[31] such that a positive force, F, corresponds to compression, positive δ, of the PEG coating and a negative force corresponds to tension of the PEG coating). The PEG coating is either modeled as an ensemble of discrete "chains" or as a film. In the former case, the term "chain" is taken to represent either a single PEG molecule grafted to the substrate or a PEG multilayer in which one or more additional molecules are bound in series to the molecule grafted to the substrate to form multimolecular chains.

Figure 3b shows an example of fitting the approach section of a force-deformation curve of PEG 20K using the Alexander−de Gennes model for compression of a polymer brush.[32,33] Because such brushes are deformed (compressed) by the AFM probe a distance δ, the entropy per brush decreases due to volume constraints, resulting in a positive osmotic pressure within the brushes. In the Alexander−de Gennes model,[32,33] the ensuing repulsive force F can be well approximated by

$$F = 50k_BTR_TL_0\Gamma^{3/2}\exp[-2\pi(1-\delta/L_0)] \qquad (1)$$

where k_B is Boltzmann's constant, T is temperature, R_T is the tip radius, L_0 is the brush height, and Γ is the grafting density in chains/area. In this model, L_0 and Γ are the fitting parameters, and eq 1 is valid only in the range $\delta/L_0 = 0.1-0.8$.[34,35] For chains formed from molecular monolayers grafted to the substrate, L_0 must be bound by $R_g < L_0 < L_C$, tending to the latter as the grafting density increases. Conversely, for chains formed from molecular multilayers, L_0 can exceed the contour length of a single chain, such that $L_0 > L_C$. In addition, it is important to note that the model assumes that the grafted chains within a brush do not overlap or entangle as they are compressed. As a result, eq 1 is well suited for modeling polymer brushes with medium grafting densities ($\approx(0.1-10)$ chains/100 nm²) in good solvents.[35]

The measured force-deformation behavior is well described by the model over the majority of the approach section. The value of L_0 in this case was ~80 nm, and this was used to set the maximum deformation point for the PEG and the abscissa scale. The statistics of the fit parameters L_0 and Γ from the complete set of force-deformation measurements over the probed area are shown in Figure 4. From these histograms, a typical brush height of between 20 and 50 nm is deduced, which is approximately the height of the PEG 20K islands observed in Figure 1 and is less than the contour length of 192
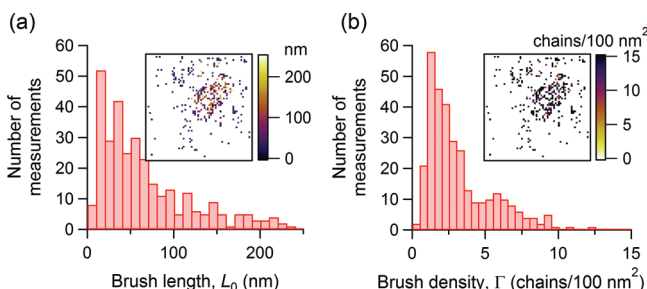
3141

dx.doi.org/10.1021/jp211256f | J. Phys. Chem. B 2012, 116, 3138–3147

Figure 4. Histograms of the (a) length and (b) grafting density of a PEG 20K brush in solution as obtained from fitting the approach sections of the force-deformation curves on PEG by the brush model; the investigated area was 500 nm ×500 nm with a spatial resolution of 7.8 nm/pixel. In the insets, the 2D spatial distributions of the fit parameters are shown.

nm for PEG 20K. Some of the brush heights given in the histogram, however, are greater than the contour length, suggesting that some brushes consisted of molecular multilayers. The typical grafting density, as found from Figure 4b, ranges from 1 to 3 chains/100 nm², which corresponds to a medium brush density with roughly 10−6 nm between grafting sites, respectively. As previously stated, L_0 must be bound by $R_g < L_0 < L_C$ for single PEG molecules, tending to the latter as the grafting density increases: The typical brush heights, which are much larger than R_g and much smaller than L_C, are consistent with a medium brush density. In addition to the quantitative characterization, the fit results also provide a clear delimitation of the PEG regions in the probed area, as can be observed in the spatial distribution maps shown in the insets of Figure 4. Further examination of the insets shows a correlation between L_0 and Γ: brush heights are greater where brush densities are smaller, implying that molecular multilayers for the PEG 20K are sparse.

In the inset of Figure 3b is shown the fit to the same approach curve as above, using the Xu and Pharr modification[36] to the Hertzian contact model[37] of an elastic continuum. In this model, the PEG chains are assumed to interact strongly to form an elastically isotropic material described by two elastic constants, allowing elastic modulus and film thickness to be determined from indentation force-deformation curves. The applied force, F, varies with the tip−sample deformation, δ, by

$$F = \frac{4}{3} E^* R_T^{1/2} \delta^{3/2} \tag{2}$$

where E^* is the reduced elastic modulus of the tip and sample. To account for the different constituents that form the sample, the reduced elastic modulus of the PEG coating−Au substrate composite was calculated on the basis of the Xu and Pharr[36] model, which utilized a first-order elastic perturbation method to consider the different elastic properties of the thin surface layer. The reduced elastic modulus was given by

$$\frac{1}{E^*} = \frac{1}{2}[1 - \nu_s + (\nu_s - \nu_f)I_1]\left[\frac{2(1 + \nu_s)}{E_s}(1 - I_0)\right.$$
$$\left. + \frac{2(1 + \nu_f)}{E_f}I_0\right] \tag{3}$$

where ν_f and ν_s are the Poisson's ratios of the film and substrate, and E_f and E_s are the Young's moduli of the film and substrate, respectively. The two weighting functions

$$I_0(\xi) = \frac{2}{\pi}\arctan\xi + \frac{1}{2\pi(1 - \nu_s)}\left[(1 - 2\nu_s)\xi\ln\frac{1 + \xi^2}{\xi^2}\right.$$
$$\left. - \frac{\xi}{1 + \xi^2}\right] \tag{4}$$

and

$$I_1(\xi) = \frac{2}{\pi}\arctan\xi + \frac{\xi}{\pi}\ln\frac{1 + \xi^2}{\xi^2} \tag{5}$$

depend through the parameter $\xi = t/a$ on the film thickness t and the contact radius $a = (\delta R_T)^{1/2}$. Here, E_f and t are the fitting parameters. In eqs 2 and 3, the tip was assumed to be rigid, and its contribution to E^* was neglected. The assumed values for the elastic parameters of the gold substrate were $E_s = 80$ GPa and $\nu_s = 0.40$, and for the Poisson's ratio of the PEG film, $\nu_f = 0.30$. Because considerable deformation of the coating is required for the molecular density to be great enough for the molecules to interact significantly and behave as a continuous film, t will be bounded by $t < L_0$, and t is expected to scale with L_0 in the case of molecular multilayers.

As shown in Figure 3b, two distinct indentation contact regions could be discerned and fit: region I and region II. In region I, the indentation fit indicated a PEG film with thickness of $t^{\text{region I}} = 75$ nm with an elastic modulus of $E_f^{\text{region I}} = 0.09$ MPa. In region II, the fit indicated a film thickness of $t^{\text{region II}} = 5$ nm and an elastic modulus of $E_f^{\text{region II}} = 1.0$ MPa. Thus, farther from the substrate, the response is that of a compliant film, about 75 nm thick and with an elastic modulus of ∼0.1 MPa. Within the last 5 nm above the substrate, the indentation response is that of a stiffer film with an elastic modulus of about 1.0 MPa. These fitting results indicate two different types of PEG morphologies, with extended chains in region I and constrained chains in region II. A similar interpretation, with two distinct elastic regions for the indentation of a hydrated PEG film in saline solution, was considered previously;[21] however, because the contribution of the substrate was not considered, the elastic moduli for the two regions were ∼1 order of magnitude greater than the values above.

The retract sections of the force-deformation curves in Figure 3c exhibited both single (in the main graph) and multiple (in the inset graph) instabilities, each characterized by a pull-off force, F_p, and a pull-off separation, L_p. The statistics of the instabilities are shown in Figure 5 as histograms and 2D image plots. Comparison of Figures 4 and 5 shows a correlation between the measured brush height, L_0, and the initial pull-off separation $L_p^{(1)}$: At locations where the brush height was large, as inferred from compression measurements, particularly where the brush was composed of a molecular multilayer, the initial tensile pull-off separation was also large. $L_p^{(1)}$ tended to be less than L_0, consistent with the idea that on initial approach, the tip senses the maximum extent of a brush, but during contact and compression, a brush can adhere to the tip at a location besides the end of a molecule. Hence, on retraction, the pull-off separation is determined by this location, and $L_p^{(1)} < L_0$.

Also shown in Figure 5 is a histogram of the maximum observed pull-off force, $F_p^{(max)}$. The width of the pull-off force distribution is significantly narrower than the pull-off separation
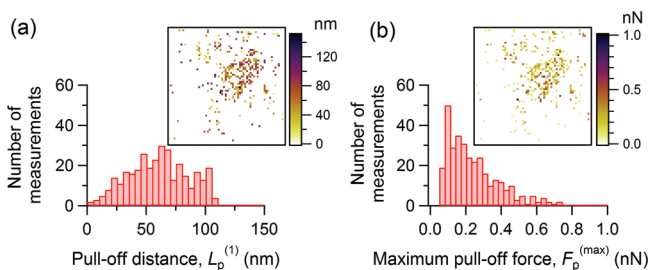
Figure 5. Histograms of the (a) first pull-off distance and (b) maximum pull-off force of a PEG 20K brush in solution as obtained from the retract sections of the force-deformation curves; the investigated area was 500 nm ×500 nm with a spatial resolution of 7.8 nm/pixel. In the insets, the 2D spatial distributions of the parameters are shown.

distribution, suggesting that the attachment mechanism between the chain and tip was relatively invariant and probably caused by a particular monomeric interaction. In addition, the typical values for $F_P^{(max)}$ ranged from 0.1 to 0.3 nN, which are indicative of pull-off forces for *single* polymeric chains.[35,38,39]

Figure 3c shows examples of fitting the retract sections of the force-deformation curves of PEG 20K with the wormlike chain (WLC) model, which represents chains as thin, elastic rods with continuous curvature and a correlation length.[40,41] In the WLC model, the applied force F is related to the separation of the attachment points, $L = L_{F=0} - \delta$, by[40,41]

$$F = -\frac{k_B T}{b}\left[\frac{L}{L_E} + \frac{1}{4(1 - L/L_E)^2} - \frac{1}{4}\right] \tag{6}$$

where $L_{F=0}$ is the separation of the attachment points at $F = 0$ prior to retraction, L_E is the maximum separation of the attachment points, and b is the persistence length. For sections of a chain shorter than b, the orientation of the chain is correlated. For single molecules grafted to the substrate and adhering to the tip, L_E must be bound by $R_g < L_E < L_C$. Conversely, for molecular multilayers, L_E can exceed the contour length, such that $L_E > L_C$.

Both single and multiple detachment events were well fitted by the WLC model. In the examples, the detachments were characterized by L_E ranging from 50 to 80 nm (64 nm in the single rupture in the main figure, and 51, 53, 58, 71, and 83 nm in ruptures 1−5 in the inset). For these rupture events, $R_g < L_E < L_C$, signifying single molecular, not molecular multilayer, interactions with the probe tip. In addition, for all of the WLC fits in Figure 3c, $b = 0.38$ nm, except for the shortest rupture ($i = 1$) in the inset, for which $b = 0.25$ nm. The results are in good agreement with the persistence length for a single PEG molecule, $b = 0.38$ nm.[42]

PEG 5K Force Spectroscopy. As with PEG 20K, the mechanical response of PEG 5K brushes on gold substrates was investigated via force spectroscopy over small areas. Different force-deformation responses from the force spectroscopy investigation are shown in Figure 6a.

The compression of PEG 5K under the AFM tip was interpreted with the Alexander−de Gennes model;[32,33] the fit results for one approach curve are shown in Figure 6b. The statistics of the fit parameters L_0 and Γ from the force-deformation measurements over the probed area are shown in Figure 7. From these histograms, a typical brush height of between 15 and 40 nm is deduced, which is about the height of the PEG 5K islands observed in Figure 2. As with the PEG 20K,
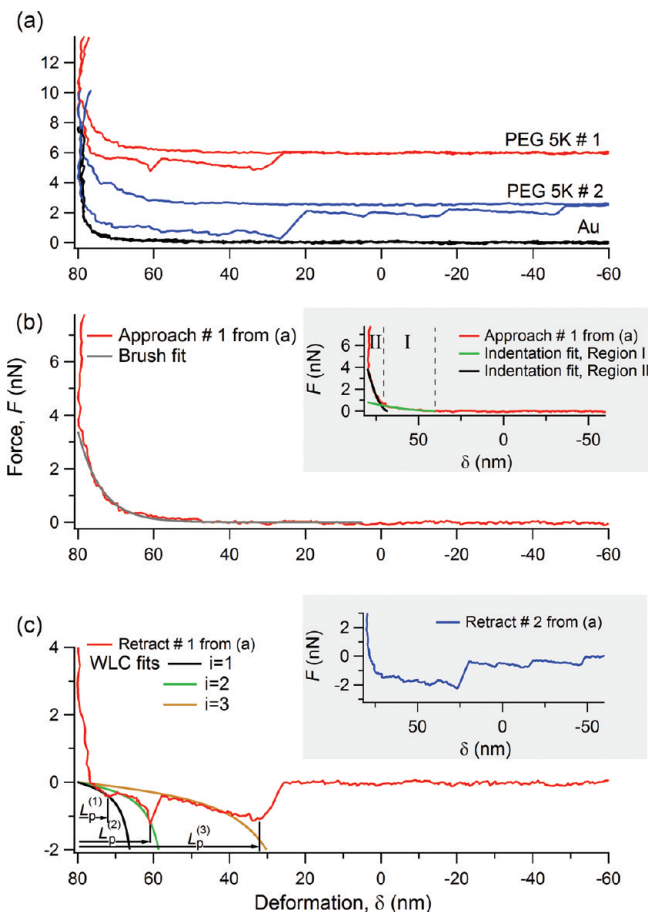

Figure 6. (a) Force-deformation curves on PEG 5K and the bare gold substrate in solution; the curves were aligned horizontally such that the upper, substrate contact, sections of the responses were aligned and then separated vertically for clarity. (b) The approach section of curve 1 is analyzed in terms of the Alexander−de Gennes brush model and the Xu and Pharr film−substrate model (inset). (c) The retract section of curve 1 is analyzed in terms of the WLC model.
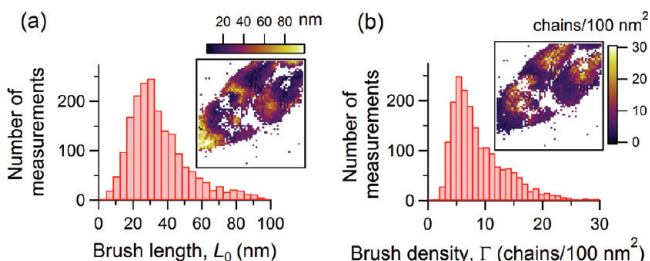

Figure 7. Histograms of the (a) length and (b) grafting density of a PEG 5K brush in solution as obtained from fitting the approach sections of the force-deformation curves on PEG by the brush model; the investigated area was 500 nm ×500 nm with a spatial resolution of 7.8 nm/pixel. In the insets, the 2D spatial distributions of the fit parameters are shown.

some of the PEG 5K brush heights are greater than the PEG 5K contour length of 47.9 nm, suggesting molecular multilayers. The typical grafting density ranges from 4 to 8 chains/100 nm², which corresponds to a medium to dense brush density with roughly 5−3.5 nm between grafting sites, respectively. The comparison between the fit parameters L_0 and Γ of the Alexander−de Gennes model for PEG 20K and PEG 5K suggests that PEG brushes have a different morphology,

depending on their molecular weight. Figures 4 and 7 suggest that L_0 for PEG 20K is slightly larger than that for PEG 5K, but Γ for PEG 20K is substantially reduced compared with that of PEG 5K. Therefore, as the molecular weight decreases, PEG chains form relatively longer, denser brushes (i.e., $L_0 \rightarrow L_C$ and Γ increases); it is conceivable that for larger molecular weights, the molecular conformation of PEG islands is in the form of mushrooms rather than brushes.[15]

The compression of PEG 5K under the AFM tip was also interpreted with the Xu and Pharr model for an indented film–substrate composite;[36] a fit to the same approach curve as above is shown in the inset of Figure 6b. As with the PEG 20K, two distinct indentation contact regions could be discerned and fit. In region I, the fit indicated a film thickness of $t^{\text{regionI}} = 40$ nm with an elastic modulus of $E_f^{\text{regionI}} = 0.20$ MPa. In region II, the fit indicated a film thickness of $t^{\text{regionII}} = 6$ nm with an elastic modulus of $E_f^{\text{regionII}} = 2.4$ MPa. For both regions, the PEG 5K values for E_f are about twice the PEG 20K values for E_f, indicating that the overall mechanical response of the PEG 5K "film" is stiffer than that of the PEG 20K "film." Therefore, as the molecular weight decreases, E_f increases, which is consistent with the increase in Γ.

In addition, comparison of Figures 3b and 6b shows that the Alexander–de Gennes brush compression model is a slightly better fit to the PEG 20K response than the PEG 5K response over the approach range, whereas the Hertzian contact model is a slightly better fit to the PEG 5K than the PEG 20K. These observations are consistent with the idea that the PEG 20K takes on a more sparse, brushlike structure, and the PEG 5K takes on a more dense, filmlike structure. The statistical results of the film analysis for PEG 5K are shown in Figure 8. As illustrated in Figures 7 and 8, $t < L_0$ and t scales with L_0, which is expected when modeling discrete chains as an elastic continuum.
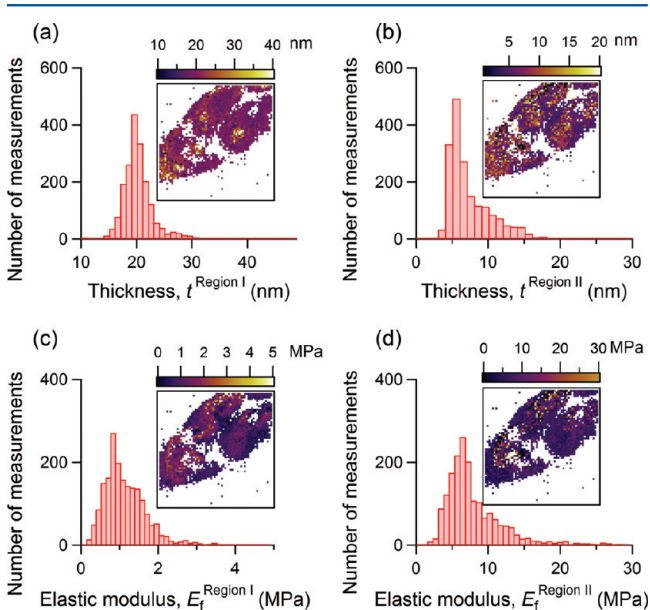

Figure 8. Histograms of the (a, b) thickness and (c, d) elastic modulus of a PEG 5K film in solution as obtained from fitting the approach sections of the force-deformation curves on PEG to the film–substrate model. The investigated area was 500 nm × 500 nm with a spatial resolution of 7.8 nm/pixel. In the insets, the 2D spatial distributions of the fit parameters are shown.

The retract sections of the force–deformation curves exhibited multiple instabilities, each described by F_p and L_p. The statistics of the instabilities are shown in Figure 9 as
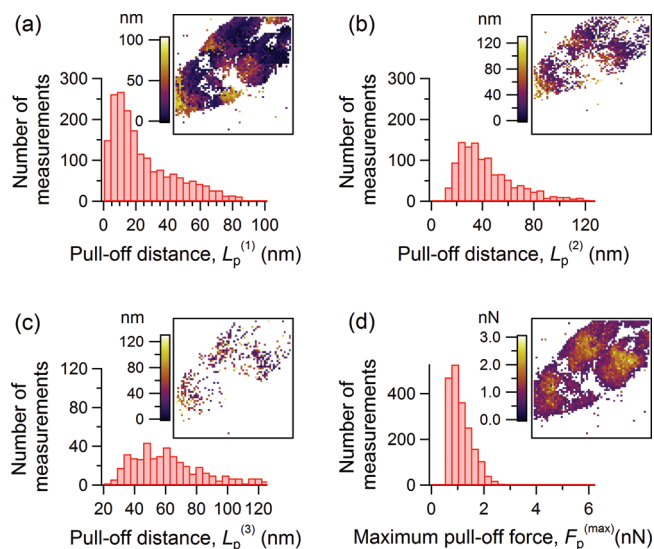

Figure 9. Histograms of the (a–c) pull-off distances and (d) maximum pull-off force of a PEG 5K brush in solution as obtained from the retract sections of the force-deformation curves. The investigated area was 500 nm × 500 nm with a spatial resolution of 7.8 nm/pixel. The index numbers represent the first (1), second (2), and third (3) rupture events. In the insets, the 2D spatial distributions of the parameters are shown.

histograms and 2D image plots of the measured pull-off separations from the first three instabilities; an example of these pull-off separations is marked on the retract response shown in Figure 6c. Comparison of Figures 7 and 9 again shows a correlation between L_0 and $L_p^{(1)}$: as L_0 increases, $L_p^{(1)}$ increases. In addition, where $L_p^{(1)}$ is large, there tends to be subsequent pull-off events at larger separations, $L_p^{(2)}$ and $L_p^{(3)}$. Also shown in Figure 9 is a histogram of the maximum pull-off forces, $F_p^{(\text{max})}$. The magnitudes of the pull-off forces were approximately an order of magnitude or greater than the 0.1–0.3 nN observed in the measurements of the PEG 20K and elsewhere.[35,38,39]

Figure 7c shows an example of fitting the retract section of the force-deformation curve of PEG 5K with the WLC model.[40,41] The values for b were fixed at 0.03, 0.02, and 0.005 nm for the first, second, and third rupture events, respectively, and L_E was used as the fitting parameter, which resulted in values of 11.2, 24.4, and 85.7 nm for the first, second, and third rupture events, respectively. For the first and second rupture events, the fitted values for L_E show that $R_g < L_E < L_C$, signifying single molecular interactions with the probe tip. Conversely, for the third rupture event, $L_E > L_C$, indicative of a molecular multilayer. The magnitudes of the persistence lengths were over an order of magnitude less than the 0.38 nm observed for the PEG 20K and elsewhere.[42]

■ DISCUSSION

The above AFM measurements of PEG molecules on flat gold substrates all indicate considerable heterogeneity in PEG structure and properties. Measurements of topography, phase contrast, and force spectroscopy demonstrate that the PEG molecules form brushlike islands distributed on the substrate, which are themselves heterogeneous in their surface coverage

and consequent mechanical properties. Three different models were used to interpret the force spectroscopy measurements: two in compression as the AFM probe approached and subsequently compressed the PEG molecules and one in tension as the probe was retracted and placed the PEG molecules in tension. Different parameters characterizing the PEG coverage and properties were extracted from each model. In particular, the Alexander–de Gennes molecular ensemble model of compression enabled brush height and molecular grafting density within an island to be determined, showing that both were heterogeneous within an island, and as a consequence, the resistance to brush compression was also heterogeneous. This observation was consistent with results obtained by analyzing the compressive responses as those of a continuous film on a substrate, as described by the Xu–Pharr modification of the Hertzian contact model, which indicated heterogeneity in both apparent film elastic modulus and thickness. In both models, the picture that emerges is that of a PEG layer that increasingly resists compression as the probe approaches the substrate. In the molecular ensemble model, the decreased entropy of the confined chains leads to an exponential increase in the compressive force, whereas in the film on substrate model, the increased density of the chains leads to an increase in the apparent modulus and a decrease in the apparent film thickness. Interpretation of the WLC model for the PEG in tension requires greater consideration.

During contact of the AFM probe tip with the PEG coating, some PEG chains can adhere to the probe tip, most likely via van der Waals interactions. On retraction of the probe, these chains are stretched between the grafted end and the end adhering to the tip, generating a force resisting probe retraction. This force increases until the stiffness of the stretched chains exceeds the stiffness of the AFM cantilever, at which point the linkage fails, probably by rupture of the weak adhesive bonds between the chains and the tip. Such detachments are commonly observed during probe-polymeric chain separation.[35,38,39]

Different scenarios, involving single or multiple detachments or pull-off events, are likely to take place: (1) A single chain is stretched, and there is one detachment if the chain is attached to the tip in just one place or multiple detachments if various segments of the chain are attached to the tip and released successively during retraction. After each rupture event, the pull-off force reverts completely to zero (zero cantilever deflection) as the deformation is either permanently or momentarily released. (2) Several chains with significant differences in length are attached to the tip such that during retraction, only the chain with the shortest length is stretched at a given time. On rupture of this chain, the force reverts to zero until the next chain begins to stretch. (3) Several chains with no significant differences in length are attached to the tip, and all are stretched in parallel as the tip is retracted; the chains can be singly or multiply attached to the tip. At any detachment but the last, the resistive force does not revert completely to zero as the remaining chains remain under tension. (4) Several groups of chains, each of which is composed of chains with no significant differences in length, are attached to the tip, and all chains within a single group are stretched in parallel as the tip is retracted, as in scenario 3. However, at a rupture event, the force reverts to zero until the next group of chains with longer lengths begins to stretch, as in scenario 2. Schematic representations of the above scenarios are illustrated in Figure 10a–d, respectively.
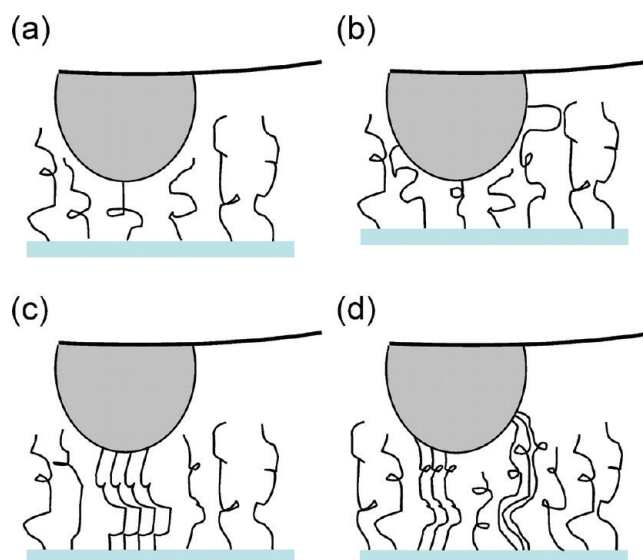

Figure 10. Schematic diagrams of the interactions between an AFM probe tip and PEG surface coating. In tension, different scenarios involving single or multiple attachments are likely to take place: (a) a single chain is attached; (b) several chains with significant differences in lengths are attached; (c) several chains with no significant differences in length are attached; and (d) several chains with and without significant differences in length are attached.

In scenario 1 above, $b = 0.38$ nm, appropriate for a single PEG molecule.[42] For a single attachment to the tip, the force–separation behavior is described by eq 6. The pull-off force, F_p, observed at detachment occurs at a separation of L_p, which is bound by the condition of $L_p < L_E$ due to the finite stiffness of the cantilever. For multiple attachments, the force–separation behavior follows a sequence of responses, each of which is independently described by eq 6 with increasing values of L_E—$L_E^{(1)} < L_E^{(2)} < L_E^{(3)}$, for example—and thus increasing values of L_p, $L_p^{(1)} < L_p^{(2)} < L_p^{(3)}$. If attachments between the tip and the PEG molecule are determined by the same physicochemical interaction, independent of the number of attachments, say, by van der Waals interaction between a PEG monomer and the tip, then the pull-off force will be the same for all $L_p^{(i)}$, that of a single attachment $F_p^{(single)}$.

In scenario 2 above, the persistence length remains at $b = 0.38$ nm, because only a single chain is stretched at any instant. In this case, the force–separation behavior always follows a sequence of responses, each of which is independently described by eq 6 with increasing values of L_E and, thus, increasing values of L_p. As in scenario 1, the pull-off force will be the same for all $L_p^{(i)}$, $F_p^{(single)}$.

In scenario 3 above, the overall force–separation behavior is given by summing the individual force–separation responses of chains in parallel, each described by eq 6 with similar values of L_E and, thus, L_p. If the L_E values are all very close, the net force is well approximated by N times the right side of eq 6, where N is the number of chains in parallel. The entire group of chains is then described by an effective persistence length, $b_{eff} = b/N$. Physically, the smaller effective persistence length reflects a decreased correlation between the orientations of segments in the separate parallel chains. In this scenario, the pull-off force is given by the chains-in-parallel upper bound, $NF_p^{(single)}$.

In scenario 4 above, the net force–separation behavior of the chains with similar lengths is given by summing the individual force–separation responses, as in scenario 3. As such, the entire

group of chains is described by an effective persistence length b/N; however, as in scenario 2, the net force-separation behavior follows a sequence of ruptures, each with a different value of L_E, and thus a different value of L_p, and a different value of b_{eff} because the number of chains in each group differs. The pull-off force for each rupture event is given by $NF_p^{(single)}$, where N is now the number of chains in each *group*. The maximum pull-off force, $F_p^{(max)}$, attained during the entire retraction is determined by the group of chains with the greatest N, but the position of the maximum in the sequence of ruptures is determined by L_E for that group.

The persistence lengths for the PEG 20K were consistent with that for a single PEG molecule, $b = 0.38$ nm,[42] and the maximum pull-off forces were predominantly in the range 0.1−0.3 nN (Figure 5b), consistent with that for single molecule adhesion.[35,38,39] In addition, when multiple instabilities were observed during probe retraction, all the pull-off forces were similar and in this range (Figure 3c, in the inset). These observations suggest that pull-off of the probe from PEG 20K brushes was as in scenario 1 or 2; that is, with a single PEG molecule or multiple PEG molecules of different attached lengths adhering to the probe. Conversely, the magnitudes of the pull-off forces for the PEG 5K were approximately an order of magnitude greater than the 0.1−0.3 nN observed in the measurements of the PEG 20K and elsewhere, in which it was clear that there was single molecule attachment.

If the attachment mechanism for the PEG 5K chains and the tip is similar to that acting in the PEG 20K experiments, the magnitudes of the pull-off forces in Figure 9 imply that multiple PEG 5K chains are attached to the tip in parallel, as in scenarios 3 and 4. In fact, for $R_T = 31$ nm and $\Gamma = 4-8$ chains/100 nm², the tip contacts about 120−200 chains, suggesting that, indeed, parallel attachments can form. Hence, each pull-off event in Figure 6c would be described by an effective persistence length less the single molecule value, and on the basis of the magnitudes of the pull-off forces in Figure 9, b_{eff} would be about 1−2 orders of magnitude less than this value. Assuming that each rupture event in Figure 6c can be described by $b_{eff} = b/N$, as in scenario 4, the values for b_{eff} used above (0.03, 0.02, and 0.005 nm for the first, second, and third rupture events, respectively) would translate to about 110 chains attached to the tip, which is in good agreement with the calculations for tip−molecule interactions. For this particular force-deformation curve, F_p increased and b_{eff} decreased for successive rupture events, which points to an increase in the number of chains stretched in parallel. However, this is not always observed, as shown in the inset of Figure 6c, where F_p decreases and b_{eff} increases for successive rupture events.

In analyzing the data, it was assumed that any long-range electrostatic interactions have a negligible contribution to the tip−PEG interfacial forces, since there are no significant repulsive forces at separations greater than the contour lengths for PEG 20K and PEG 5K (see Figures 3 and 6) and the values for L_0, t, L_p, and L_E are different for PEG 20K and PEG 5K (see Figures 3−9). If long-range electrostatic interactions existed, they would likely occur at separations much larger than L_C, which would likely change the values for L_0, t, L_p, and L_E such that the PEG 20K and PEG 5K surface coatings would appear to have similar characteristics. In a previous study, it was indeed shown that end-grafted PEG brushes of moderate to long chain length exhibit no long-range electrostatic interactions and only small ionic strength dependence.[43]

■ SUMMARY AND CONCLUSIONS

In summary, the morphology and mechanical properties of thiol-functionalized PEG 5K and PEG 20K grafted onto flat gold substrates were elucidated from a statistical analysis of force spectroscopy data in aqueous PEG solution. A constitutive description of the brush organizations and mechanical responses of the two biotechnologically relevant PEG molecular weights was provided from analysis of the approach and retract sections of force−deformation curves. Various models were used to describe the mechanical response of the PEG coatings in compression and tension. In compression, the models showed that PEG chains form relatively longer, denser brushes (i.e., $L_0 \rightarrow L_C$ and Γ increases) with larger elastic moduli (E_f increases by a factor of 2) as the molecular weight decreases. In tension, the PEG chains adhere to the probe tip in different configurations, depending on the molecular weight; PEG 20K chains are attached to the tip predominantly as single chains, as in scenario 1 or 2, whereas PEG 5K chains are attached to the tip predominantly as groups of chains as in scenario 4. Collectively, the AFM and force spectroscopy results reveal significant heterogeneity in PEG surface coverage and properties within individual PEG islands.

By examining a planar gold surface as a model nanoparticle with an infinite radius of curvature, quantifying the mechanical properties of PEG surface coatings on gold surfaces is now demonstrated with the intent that the high spatial resolution of AFM will facilitate previously unattainable studies on actual nanoparticles. The densities of PEG 5K and PEG 20K observed here are well within an order of magnitude of those inferred from the integrative techniques of infrared spectroscopy and electrospray differential mobility analysis of PEG functionalized 60 nm gold nanoparticles in aqueous solution.[44]

PEG-functionalized gold nanoparticles are presently used for applications such as "immunogold" targeted labeling for human carcinoma tissue because the presence of surface-bound thiol-functionalized PEG has been demonstrated to resist direct physisorption of proteins onto the surface of nanoparticles, thus enhancing biocompatibility.[8,45] As a result of its growing clinical use, it is important to know both the adsorbed density and the structural form of thiol-functionalized PEG on the surface of particles, because these are indicators of therapeutic performance.[46]

In addition, with the new ability to map PEG properties on single nanoparticles, the technique presented in this work can address key questions when developing quality control measurements and batch-to-batch consistency for gold nanoparticle based nanomedicines, such as whether all nanoparticles are uniformly coated with submonolayers or if two populations (completely coated and uncoated) exist.[44,47,48] This measurement approach can provide increased certainty to answering potentially limiting regulatory questions when advancing nanomedicines through clinical trials.

Finally, this work also suggests that when functionalizing gold nanoparticles with thiol-functionalized PEG 5K or PEG 20K using the typical reaction conditions reported from the literature for alkylmonothiols,[49,50] low and nonuniform coverage densities may occur if radius of curvature effects are assumed to be negligible, and characterization of large numbers of single nanoparticles through high-spatial resolution mapping experiments could provide previously unattainable confidence in the validation of integrative measurements.

3146

dx.doi.org/10.1021/jp211256f | *J. Phys. Chem. B* 2012, 116, 3138−3147

■ ASSOCIATED CONTENT

ⓢ Supporting Information

The dehydration/crystallization of PEG 20K and PEG 5K in air as observed by AFM imaging. This material is available free of charge via the Internet at http://pubs.acs.org.

■ AUTHOR INFORMATION

Corresponding Author

*Phone: (301) 975 3675. Fax: (301) 975 5995. E-mail: gheorghe.stan@nist.gov.

Notes

The authors declare no competing financial interest.

■ REFERENCES

(1) Hirsch, L. R.; Stafford, R. J.; Bankson, J. A.; Sershen, S. R.; Rivera, B.; Price, R. E.; Hazle, J. D.; Halas, N. J.; West, J. L. *Proc. Natl. Acad. Sci.* **2003**, *23*, 13549−13554.

(2) Hall, J. B.; Dobrovolskaia, M. A.; Patri, A. K.; McNeil, S. E. *Nanomedicine* **2007**, *2*, 789−803.

(3) Stern, S. T.; McNeil, S. E. *Toxicol. Sci.* **2008**, *101*, 4−21.

(4) Dreaden, E. C.; Mwakwari, S. C.; Sodji, Q. H.; Oyelere, A. K.; El-Sayed, M. A. *Bioconjugate Chem.* **2009**, *20*, 2247−2253.

(5) Dobrovolskaia, M. A.; McNeil, S. E. *Nat. Nanotechnol.* **2007**, *2*, 469−478.

(6) Loo, C.; Lowery, A.; Halas, N.; West, J.; Drezek, R. *Nano Lett.* **2005**, *5*, 709−711.

(7) Niidome, T.; Yamagata, M.; Okamoto, Y.; Akiyama, Y.; Takahashi, H.; Kawano, T.; Katayama, Y.; Niidome, Y. *Controlled Release* **2006**, *114*, 343−347.

(8) Eck, W.; Craig, G.; Sigdel, A.; Ritter, G.; Old, L. J.; Tang, L.; Brennan, M. F.; Allen, P. J.; Mason, M. D. *ACS Nano* **2008**, *2*, 2263−2272.

(9) Tracy, J. B.; Kalyuzhny, G.; Crowe, M. C.; Balasubramanian, R.; Choi, J. P.; Murray, R. W. *J. Am. Chem. Soc.* **2007**, *129*, 6706−6707.

(10) Banquy, X.; Suarez, F.; Argaw, A.; Rabanel, J.-M.; Grutter, P.; Bouchard, J.-F.; Hildgen, P.; Giasson, S. *Soft Matter* **2009**, *5*, 3984−3991.

(11) Aubin-Tam, M.-E.; Hamad-Schifferli, K. *Biomed. Mater.* **2008**, *3*, 034001.

(12) Li, D. X.; He, Q.; Zhu, H. F.; Tao, C.; Li, J. B. *J. Nanosci. Nanotechnol.* **2007**, *7*, 3089−3094.

(13) Elghanian, R.; Storhoff, J. J.; Mucic, R. C.; Letsinger, R. L.; Mirkin, C. A. *Science* **1997**, *277*, 1078−1081.

(14) Carpick, R. W.; Salmeron, M. *Chem. Rev.* **1997**, *97*, 1163−1194.

(15) Zhu, X. Y.; Jun, Y.; Staarup, D. R.; Major, R. C.; Danielson, S.; Boiadjev, V.; Gladfelter, W. L.; Bunker, B. C.; Guo, A. *Langmuir* **2001**, *17*, 7798−7803.

(16) Zdyrko, B.; Klep, V.; Luzinov, I. *Langmuir* **2003**, *19*, 10179−10187.

(17) Zdyrko, B.; Varshney, S. K.; Luzinov, I. *Langmuir* **2004**, *20*, 6727−6735.

(18) Rundqvist, J.; Hoh, J. H.; Haviland, D. B. *Langmuir* **2005**, *21*, 2981−2987.

(19) Yang, J.; Zhao, T.; Zhou, Y.; Liu, L.; Li, G.; Zhou, E.; Chen, X. *Macromolecules* **2007**, *40*, 2791−2797.

(20) Hamley, I. W.; Krysmann, M. J. *Langmuir* **2008**, *24*, 8210−8214.

(21) Suo, Z.; Arce, F. T.; Avci, R.; Thieltges, K.; Spangler, B. *Langmuir* **2006**, *22*, 3844−3850.

(22) Nnebe, I. M.; Schneider, J. W. *Macromolecules* **2006**, *39*, 3616−3621.

(23) DelRio, F. W.; Jaye, C.; Fischer, D. A.; Cook, R. F. *Appl. Phys. Lett.* **2009**, *94*, 131909.

(24) DelRio, F. W.; Steffens, K. L.; Jaye, C.; Fischer, D. A.; Cook, R. F. *Langmuir* **2010**, *26*, 1688−1699.

(25) DelRio, F. W.; Rampulla, D. M.; Jaye, C.; Stan, G.; Gates, R. S.; Fischer, D. A.; Cook, R. F. *Chem. Phys. Lett.* **2011**, *512*, 243−246.

(26) Flory, P. J.; Rehner, J. *J. Chem. Phys.* **1943**, *11*, 521−526.

(27) Hedden, R. C.; Bauer, B. J. *Macromolecules* **2003**, *36*, 1829−1835.

(28) Flory, P. J. *Statistical Mechanics of Chain Molecules*; Oxford University Press: New York, 1989, p 11.

(29) Stan, G; Ciobanu, C. V.; Parthangal, P. M.; Cook, R. F. *Nano Lett.* **2007**, *7*, 3691−3697.

(30) Jo, S.; Park, K. *Biomaterials* **2000**, *21*, 605−616.

(31) Johnson, K. L. *Contact Mechanics*, 6th ed.; Cambridge University Press: Cambridge, 1996, p 93.

(32) Alexander, S. *J. Phys. (Paris)* **1977**, *38*, 983−987.

(33) de Gennes, P. G. *Adv. Colloid Interface Sci.* **1987**, *27*, 189−209.

(34) Israelachvilli, J. N. *Intermolecular and Surface Forces*, 2nd ed.; Academic Press: London, 1992, pp 293−298.

(35) Butt, H.-J.; Kappl, M; Mueller, H.; Raiteri, R. *Langmuir* **1999**, *15*, 2559−2565.

(36) Xu, H.; Pharr, G. M. *Scr. Mater.* **2006**, *55*, 315−318.

(37) Hertz, H. *J. Reine Angew. Math.* **1881**, *92*, 156−171.

(38) Bemis, J. E.; Akhremitchev, B. B.; Walker, G. C. *Langmuir* **1999**, *15*, 2799−2805.

(39) Cuenot, S.; Gabriel, S.; Jerome, R.; Jerome, C.; Fustin, C. A.; Jonas, A. M.; Duwez, A. S. *Macromolecules* **2006**, *39*, 8428−8433.

(40) Bustamante, C.; Marko, J. F.; Siggia, E. D.; Smith, S. *Science* **1994**, *265*, 1599−1600.

(41) Marko, J. F.; Siggia, E. D. *Macromolecules* **1995**, *28*, 8759−8700.

(42) Kienberger, F; Pastushenko, V. P.; Kada, G.; Gruber, H. J.; Riener, C; Schindler, H; Hinterdorfer, P. *Single Mol.* **2000**, *1*, 123−128.

(43) Feldman, K.; Hahner, G.; Spencer, N. D.; Harder, P.; Grunze, M. *J. Am. Chem. Soc.* **1999**, *121*, 10134−10141.

(44) Tsai, D. H.; Davila-Morris, M.; DelRio, F. W.; Guha, S.; Zachariah, M.; Hackley, V. A. *Langmuir* **2011**, *27*, 9302−9313.

(45) Paciotti, G. F.; Kingston, D. G. I.; Tamarkin, L. *Drug Dev. Res.* **2006**, *67*, 47−54.

(46) Dobrovolskaia, M. A.; Patri, A. K.; Zheng, J. W.; Clogston, J. D.; Ayub, N.; Aggarwal, P; Neun, B. W.; Hall, J. B.; McNeil, S. E. *Nanomed. Nanotechnol. Biol. Med.* **2009**, *5*, 106−117.

(47) Tsai, D. H.; DelRio, F. W.; MacCuspie, R. I.; Cho, T. J.; Zachariah, M.; Hackley, V. A. *Langmuir* **2010**, *26*, 10325−10333.

(48) Tsai, D. H.; DelRio, F. W.; Keene, A. M.; Tyner, K. M.; MacCuspie, R. I.; Cho, T. J.; Zachariah, M.; Hackley, V. A. *Langmuir* **2011**, *27*, 2464−2477.

(49) Woehrle, G. H.; Brown, L. O.; Hutchison, J. E. *J. Am. Chem. Soc.* **2005**, *127*, 2172−2183.

(50) Song, Y.; Murray, R. W. *J. Am. Chem. Soc.* **2002**, *124*, 7096−7102.